Applied Catalysis B: Environmental 188 (2016) 189–197

Contents lists available at ScienceDirect

Applied Catalysis B: Environmental

journal homepage: www.elsevier.com/locate/apcatb

# Selective catalytic reduction of $NO_x$ with $H_2$ over $WO_3$ promoted $Pt/TiO_2$ catalyst

Zhiming Liu[a,*], Yunan Lu[a], Lei Yuan[a], Lingling Ma[b,*], Lirong Zheng[c], Jing Zhang[c], Tiandou Hu[c]

[a] State Key Laboratory of Chemical Resource Engineering, Beijing University of Chemical Technology, Beijing 100029, China
[b] Division of Nuclear Technology and Applications, Institute of High Energy Physics, Chinese Academy of Sciences, Beijing 100049, China
[c] Beijing Synchrotron Radiation Facility, Institute of High Energy Physics, Chinese Academy of Sciences, Beijing 100049, China

ARTICLE INFO

*Article history:*
Received 20 November 2015
Received in revised form 1 February 2016
Accepted 3 February 2016
Available online 4 February 2016

*Keywords:*
Nitrogen oxides
$H_2$-SCR
Pt-$WO_3$/$TiO_2$ catalyst

ABSTRACT

$Pt/TiO_2$ and $WO_3$ modified $Pt/TiO_2$ catalysts have been investigated for the selective catalytic reduction of $NO_x$ by $H_2$ ($H_2$-SCR) in the presence of oxygen. It was found that the addition of $WO_3$ leads to a significant promoting effect on the low-temperature activity of $Pt/TiO_2$ catalyst and the optimal loading is 2%. X-ray absorption near-edge structure (XANES) revealed the electron transfer from $WO_3$ to Pt active sites, leading to the formation of metallic Pt, which is responsible for the low-temperature $H_2$-SCR of $NO_x$. In-situ DRIFTS demonstrated that the introduction of $WO_3$ to Pt catalyst not only contributes to the formation of reactive adsorbed $NO_x$ species on the catalyst, but also promotes the formation of $NH_4^+$ species. All of these factors, collectively, account for the improved low-temperature activity of Pt-$WO_3$/$TiO_2$ catalyst.


## 1. Introduction

Nitrogen oxides ($NO_x$) emitted from both mobile and stationary sources can cause various environmental problems, such as the formation of acid rain as well as photochemical smog [1]. Selective catalytic reduction(SCR) of $NO_x$ with different reducing agents is one promising technology for the abatement of $NO_x$ in the presence of oxygen [2–4]. In the $NH_3$-SCR of $NO_x$, many problems are encountered, such as catalyst deterioration and "$NH_3$ slip" [5]. For the HC-SCR, the poor low-temperature activity remains to be solved [6,7]. $H_2$-SCR offers a solution to these problems since in this process $H_2$ can efficiently reduce $NO_x$ at relatively low temperatures [8–10]. Moreover, zero emissions of greenhouse gas in the reaction make it environmentally benign. For diesel powered vehicles, on-board hydrogen generation can be achieved by reforming of diesel fuel [11]. Therefore, $H_2$-SCR has attracted more and more attention as alternative de$NO_x$ route to $NH_3$-SCR and HC-SCR for the removal of $NO_x$ emitted from diesel powered vehicles.

Previous research demonstrated that supported Pt catalyst is active for the $H_2$-SCR of $NO_x$ [12–14]. In terms of cost, the catalyst with low Pt loading is preferred. Typical exhaust temperature of high efficiency gas boilers and diesel passenger cars are below 200 °C [15,16]. For Pt catalyst with low Pt content, its de$NO_x$ activity at low temperatures (<200 °C) needs to be improved.

Some promoters have been employed to improve the $H_2$-de$NO_x$ performance of Pt catalyst. The addition of Cr to Pt/ZSM-35 catalyst resulted in an activity enhancement. The promoting effect of Cr is due to the improved $NO_x$ adsorption and the promoted generation of $NH_x$ species [17]. Compared with $Pt/SiO_2$ catalyst, Pt-Mo-Na/$SiO_2$ showed higher activity and $N_2$ selectivity for $H_2$-SCR. The higher catalytic performance was attributed to its poor oxygen affinity in comparison with $Pt/SiO_2$ [18]. Burch et al. [19] reported that small addition of Na remarkably improved the $NO_x$ conversion while larger loadings of Na have a severe poisoning effect on $Pt/Al_2O_3$ catalyst. The optimum Na loading is about 0.27%. On the other hand, Machida [20] found that the optimal Na loading is 15% in the case of Na as a promoter for Pt-ZSM-5 catalyst. DRIFT studies revealed that the function of Na is promoting the formation of $NO_3^-$, a key intermediate in the $H_2$-SCR of $NO_x$. The above reports indicate that the effect of promoter on the aim reaction is dependent on the types of the support. Kureti et al. [15] found that $WO_3$ showed a promoting effect on $Pt/ZrO_2$ for the $H_2$-SCR. However, poisonous $NH_3$ was prone to be formed in the $H_2$-SCR of $NO_x$ in the case of $ZrO_2$ as the support of Pt [21].

In the present study, the effect of $WO_3$ on the catalytic performance of $Pt/TiO_2$ has been investigated. The added $WO_3$ showed a promoting effect on the activity of $Pt/TiO_2$ catalyst for the

* Corresponding authors.
*E-mail addresses:* liuzm@mail.buct.edu.cn (Z. Liu), malingling@ihep.ac.cn (L. Ma).

http://dx.doi.org/10.1016/j.apcatb.2016.02.008
0926-3373/

$H_2$-SCR, and the activity temperature window was shifted to the low-temperature range (100–175 °C), which is useful for the low-temperature de$NO_x$, such as under automotive "cold-start" conditions. In the presence of $H_2O$, the promoting effect of $WO_3$ is more noticeable. Catalyst characterization and in situ DRIFTS studies were performed to get insight into the origin of the promoting effect of $WO_3$.

## 2. Experimental

### 2.1. Catalyst preparation

Catalysts were prepared by the incipient wetness impregnation method, and Degussa AEROSIL $TiO_2$ P25 was used as the support. 0.5%Pt/$TiO_2$ (Pt0.5) was prepared by impregnating $TiO_2$ with $H_2PtCl_6$ solution, stirred for 4 h, then dried at 120 °C for 6 h and calcined at 500 °C for 4 h in air. For a series of 0.5%Pt-x$WO_3$/$TiO_2$(Pt0.5Wx, x represents the weight percentage of $WO_3$) catalysts, first impregnating $TiO_2$ with $(NH_4)_{10}W_{12}O_{41}$ and oxalic acid solution, stirred for 4 h and dried at 120 °C for 6 h, then the obtained power was impregnated with $H_2PtCl_6$ solution, stirred for 4 h and dried at 120 °C for 6 h, subsequently calcined at 500 °C for 4 h in air.

### 2.2. Evaluation of the catalytic performance

The catalytic performance tests were conducted in a fixed-bed quartz reactor. The reaction conditions were controlled as follows: 0.25% NO, 1% $H_2$, 5% $O_2$, 5%$H_2O$ (when used), 100 ppm CO (when used), 5% $CO_2$ (when used) and the balance helium. The total flow rate of the feed gas was 200 mL $min^{-1}$. A sample weight of 0.2 g was employed, corresponding to the gas hourly space velocity (GHSV) of 53,000 $h^{-1}$. The inlet and outlet gas concentrations of NO and $NO_2$ were analyzed by a chemiluminescence NO/$NO_2$ analyzer (Thermo Scientific, model 42i-HL). Meanwhile, the concentrations of $N_2O$ and $NH_3$ were monitored by a FTIR spectrometer (Gasmet FTIR DX4000). No $NH_3$ was detected in the $H_2$-SCR of $NO_x$. The $NO_x$ conversion ($C_{NOx}$) and $N_2$ selectivity ($S_{N2}$) were calculated by the following equations, respectively.

$$C_{NOx} = \frac{[NO_x]_{in} - [NO_x]_{out}}{[NO_x]_{in}} \times 100\% \quad (1)$$

$$S_{N2} = \frac{[NO_x]_{in} - [NO_x]_{out} - 2[N_2O]_{out}}{[NO_x]_{in} - [NO_x]_{out}} \times 100\% \quad (2)$$

where $[NO_x]_{in}$ and $[NO_x]_{out}$ represent the total concentration of $NO_x$ in the inlet and outlet gas, respectively, and $[N_2O]_{out}$ is the concentration of $N_2O$ in the outlet gas.

The reaction rate for $N_2$ production was obtained using the differential reactor over which the $NO_x$ conversion was kept below 20%.

$$r_{N2}\left(\mu mol/g \cdot s\right) = \frac{F_T y_{NO_x} C_{NO_x} S_{N_2}}{2W}$$

Where $F_T$ is the total molar flow rate ($\mu mol\, s^{-1}$), $y_{NOx}$ is the molar fraction of $NO_x$ in the feed, and W is the weight of catalyst (g).

### 2.3. Characterization of the catalysts

The BET surface area of the catalysts was conducted with a nitrogen adsorption apparatus (Micromeritics, ASAP 2010 M + C) by the BET method. The samples were degassed in vacuum at 300 °C for 3 h before the surface area measurement. X-ray diffraction (XRD) patterns were recorded with a Brucker D8 ADVANCE system using a Cu Kα radiation (λ = 0.15418 nm).

Temperature-programmed reduction ($H_2$-TPR) experiments were carried out on a ChemiSorb 2720 adsorption instrument. After pretreated at 300 °C for 1 h in $N_2$ flow, the sample was reduced under a 5% $H_2$ gas flow (50 mL $min^{-1}$) at a rate of 10 °C $min^{-1}$. Temperature programmed desorption of $NO_x$ ($NO_x$-TPD) was performed in a fixed bed quartz reactor. A typical sample of 0.1 g and a gas flow rate of 100 mL $min^{-1}$ were used during the experiment. Prior to the measurement, the catalyst was pretreated under helium atmosphere at 400 °C for 1 h and then cooled down to room temperature. Subsequently the catalyst was exposed to a mixture of 0.25% NO and 5% $O_2$ (balanced by helium) for 1 h. After the catalyst was purged in helium to remove the physically adsorbed species, it was heated up to 600 °C at a rate of 10 °C $min^{-1}$ in flowing He. NO and $NO_2$ concentrations were detected online by the chemiluminescence $NO_x$ analyzer.

X-ray Absorption Fine Structure (XAFS) data were measured at the beam lines 1W1B of Beijing Synchrotron radiation facility (BSRF) with an electron beam energy of 2.2 GeV and a current of 50 mA. The energy was calibrated by a platinum foil and fixed at 13273 eV. A Si (111) double crystal monochromator was used for energy scan. The catalysts analysis was performed in fluorescence mode with a Lytle detector while reference samples, including $PtO_2$ and $WO_3$, were performed in transmission mode with an ion chamber. The measurements were performed at room temperature. Because of the nearness of the Pt $L_{III}$ edge (11564 eV) to the W $L_{II}$ edge (11544 eV), the data analysis for the Pt and W was done for the Pt $L_{II}$ (13273 eV) and W $L_{III}$ (10207 eV) edges, respectively. The resultant data were analyzed by Athena from Ifeffit 0.9.20 software package (Demeter© Bruce Ravel).

In-situ DRIFTS spectra were recorded on a Fourier transform infrared spectrometer (FTIR, Thermo Nicolet 6700) equipped with a high temperature environmental cell fitted with ZnSe window and a MCT detector. The samples in the DRIFT IR cell were pretreated at 400 °C for 1 h under helium with a flow rate of 100 mL $min^{-1}$ before each experiment. Subsequently the background spectrum was collected in flowing helium. The background was subtracted from the sample spectrum obtained at the same temperature. All the spectra were taken by recording 100 scans at 4 $cm^{-1}$ resolution.

## 3. Results and discussion

### 3.1. Catalytic performance for $H_2$-SCR

The catalytic performances of Pt/$TiO_2$ and Pt-$WO_3$/$TiO_2$ catalysts for $H_2$-SCR are illustrated in Fig. 1. Introduction of $WO_3$ leads to a significant promoting effect on the activity in low temperature range of 100–175 °C. The addition of 1% $WO_3$ results in an enhancement of $NO_x$ conversion from 35 to 86% at 150 °C. With increasing the $WO_3$ loading from 1 to 2%, the activity temperature window was further shifted to the low temperature region with 88% $NO_x$ conversion achieved at 125 °C. While a slight decrease of $NO_x$ conversion can be observed as the $WO_3$ loading is further increased to 5%. The highest selectivity to $N_2$ was also obtained over Pt0.5W2 catalyst. Therefore, the optimal $WO_3$ loading for the modified Pt/$TiO_2$ catalyst is 2%. Besides $N_2$, $N_2O$ was also produced in the $H_2$-SCR of $NO_x$ as reported in the previous literature [15]. PtW alloy catalyst could be designed to improve the $N_2$ selectivity [22]. For Pt0.5W2 catalyst, the unselective combustion of $H_2$ with $O_2$ becomes predominant above 150 °C and the remaining $H_2$ for the SCR reaction is diminished, resulting in the $NO_x$ conversion decreased [8]. Previous research showed that the activity temperature window of Pt-Cr/ZSM-5 [17] and Pt/$La_{0.7}Sr_{0.2}Ce_{0.1}FeO_3$ [23] in terms of ΔT (the temperature range in which $NO_x$ conversion is higher than the half of the maximum $NO_x$ conversion) is about 90 °C and 110 °C, respectively. The present Pt0.5W2 catalyst exhibited wider operat-

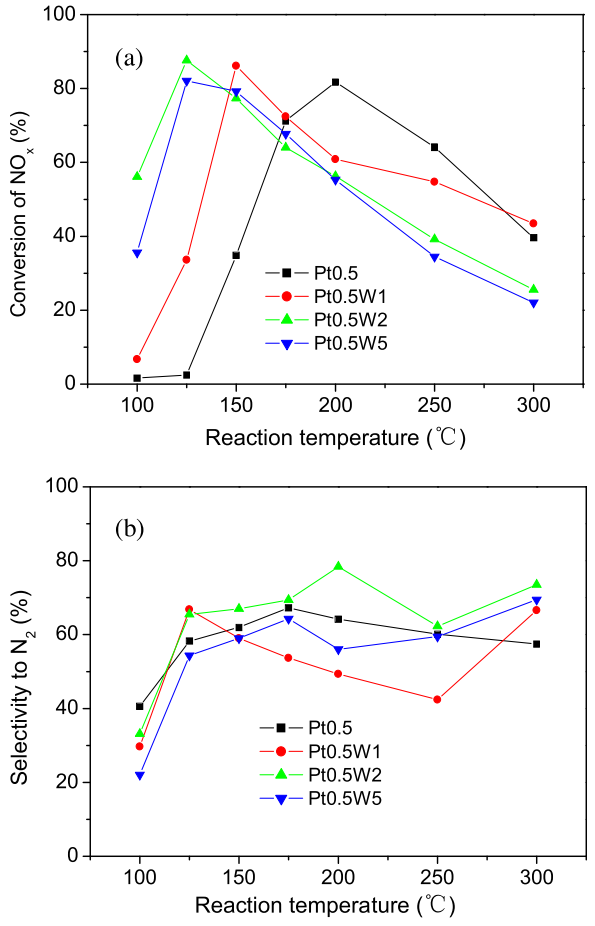


**Fig. 1.** $H_2$-SCR performances of Pt0.5 and Pt0.5Wx with different $WO_3$ loadings. (a) $NO_x$ conversion; (b) $N_2$ selectivity. Reaction conditions: 0.25% NO, 1% $H_2$, 5% $O_2$, He balance, GHSV = 53, 000 $h^{-1}$.

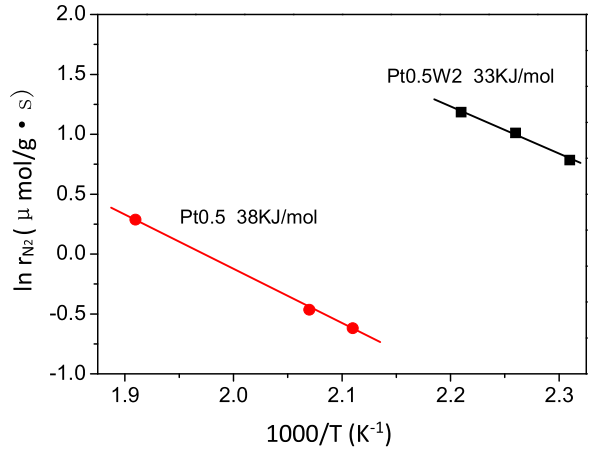


**Fig. 2.** Arrhenius plots for the formation rate of $N_2$ over Pt0.5 and Pt0.5W2 catalysts: (●) Pt0.5, (■) Pt0.5W2.

ing temperature window with ΔT of 130 °C, which is close to that of the Pt/MgO-$CeO_2$ catalyst [24]. For Pt0.5W2 catalyst its de$NO_x$ activity at high temperature needs to be improved. Alloy catalyst is stable to re-oxidation at high temperature [25] and PtW alloy catalyst can be designed to solve this drawback. Fig. 2 shows the results of Arrhenius plots for the rate of $N_2$ formation over Pt0.5 and Pt0.5W2 catalysts. It is evident that the apparent activation energy (Ea) over Pt0.5W2 catalyst is lower than that over Pt0.5 catalyst. The lower Ea value over Pt0.5W2 indicates that the $H_2$-SCR of $NO_x$

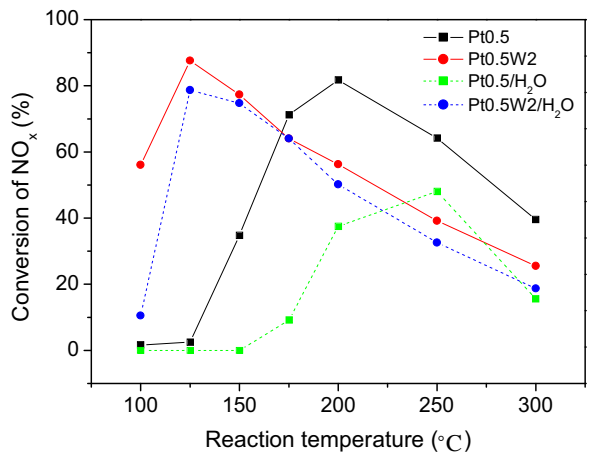


**Fig. 3.** Comparison of $H_2$-SCR activities of Pt0.5 and Pt0.5W2 catalysts in the presence of $H_2O$. Reaction conditions: 0.25% NO, 1% $H_2$, 5% $O_2$, 5%$H_2O$, He balance. GHSV = 53, 000 $h^{-1}$.

proceeds more easily than that occurs over Pt0.5 catalyst due to the addition of $WO_3$.

### 3.2. *Effect of $H_2O$*

The $H_2$-SCR activities of Pt0.5 and Pt0.5W2 catalysts in the presence of $H_2O$ were investigated and the temperature profiles of $NO_x$ conversion are presented in Fig. 3.

It is evident that the activity of Pt0.5 catalyst was seriously suppressed by the presence of $H_2O$. Only 48% maximum $NO_x$ conversion was obtained at 250 °C. The competitive adsorption between $H_2O$ and the reactants on the active site could be the reason for the $H_2O$ inhibition [26]. In contrast, the presence of $H_2O$ just showed a minor inhibiting effect above 125 °C on Pt0.5W2 catalyst, over which the maximum $NO_x$ conversion of ~80% was obtained at 125 °C. Therefore, Pt0.5W2 catalyst exhibited much higher activity than Pt0.5 in the presence of $H_2O$. Over Pt0.5W2 catalyst, besides the competitive adsorption between $H_2O$ and the reactants, the dissociation of $H_2O$ could also occur. The latter process increases the H-reservoir necessary for the reduction of $NO_x$ thus showing a positive effect [24]. These two processes lead to the higher tolerance of Pt0.5W2 catalyst to $H_2O$, which is very important in viewpoint of practical application.

### 3.3. *Effects of CO and $CO_2$*

Fig. 4(a) presents the effect of CO on the catalytic activities of Pt0.5 and Pt0.5W2 catalysts. It can be seen that the presence of CO leads to the activity loss of Pt0.5 catalyst below 250 °C, with only about 10% conversion of $NO_x$ obtained at 300 °C. As Costa et al. [13] reported, the poisoning effect of CO can be attributed to the strong CO adsorption on Pt sites which results in a significant lowering of the surface coverage of adsorbed H, and thus in the decrease of $NO_x$ conversion. For Pt0.5W2 catalyst, a drastic decline of $NO_x$ conversion was observed below 150 °C, further increasing the temperature leads to the $NO_x$ conversion sharply increased and above 175 °C the conversion is higher than that obtained in the absence of CO. At higher temperature the oxidized Pt could be reduced by CO, which would result in the increase of surface coverage of H, and thus in the increase of $NO_x$ conversion [13].

Furthermore, the effect of $CO_2$ on the activities of Pt0.5 and Pt0.5W2 catalysts was investigated as well and the results are illustrated in Fig. 4(b). Similar to the poisoning effect of CO, the presence $CO_2$ leads to the activity loss of Pt0.5 catalyst. For Pt0.5W2 catalyst, $CO_2$ caused a significant decrease of $NO_x$ conversion at 100 °C, how-

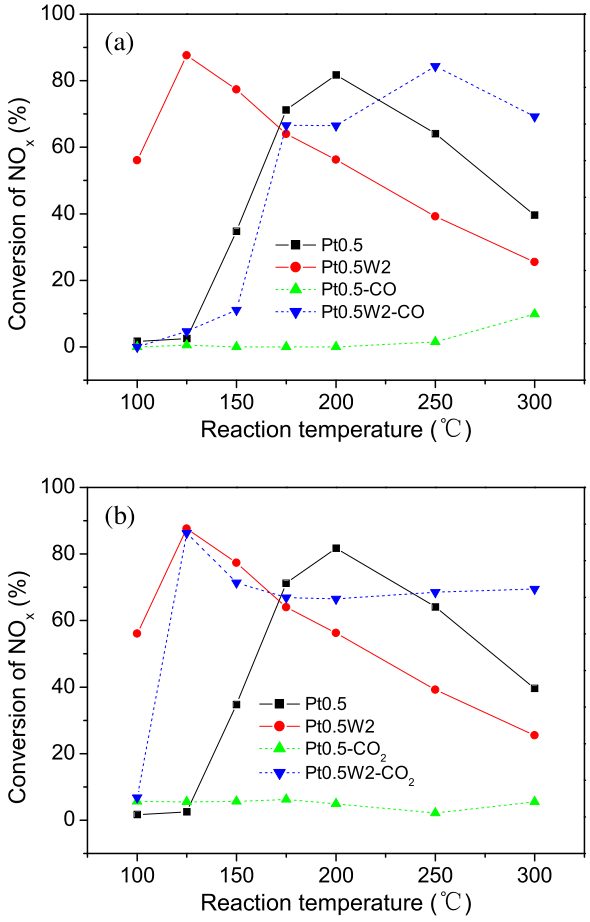


**Fig. 4.** Effects of CO (a) and $CO_2$ (b) on the $H_2$-SCR activities of Pt0.5 and Pt0.5W2 catalysts. Reaction conditions: 0.25% NO, 1% $H_2$, 5% $O_2$, 0 or 100 ppm CO, 0 or 5% $CO_2$, He balance, GHSV = 53, 000 $h^{-1}$.

ever, the inhibiting effect becomes slight in the temperature range of 125–175 °C and above 175 °C the conversion of $NO_x$ is noticeably improved. The promoting effect of $CO_2$ at high temperatures will be definitely discussed in the future investigations.

### 3.4. Effect of hydrothermal aging

Hydrothermal aging was conducted by passing a 5%$H_2O$/5%$O_2$/He gas mixture over Pt0.5 and Pt0.5W2 catalysts at 700 °C for 4 h and their $H_2$-SCR activities were investigated. As shown in Fig. 5, although the activity temperature window was shifted to higher temperatures due to the hydrothermal aging, the activity of aged Pt0.5W2 is much higher than the aged Pt0.5 catalyst. The aged Pt0.5W2 is even more active than the fresh Pt0.5 catalyst below 200 °C. Therefore, Pt0.5W2 still exhibited high activity for the $H_2$-SCR of $NO_x$ even after the accelerated aging.

### 3.5. Effects of $H_2$ and $O_2$

Previous research showed that the concentration of $H_2$ and $O_2$ is crucial for the $H_2$-SCR reaction [15,27]. Hence, the effects of $H_2$ and $O_2$ concentrations are investigated on the active Pt0.5W2 catalyst at 125 °C and the results are shown in Fig. 6. From Fig. 6(a), it can be seen that both the $NO_x$ conversion and $N_2$ selectivity were noticeably improved with increasing $H_2$ concentration from 0.5% to 1%. As reported by Burch and Coleman [28], as the surface coverage with $H_{ads}$ increases the dissociation of NO is accelerated, leading to an increase in $NO_x$ conversion and an enhanced selectivity to $N_2$. The

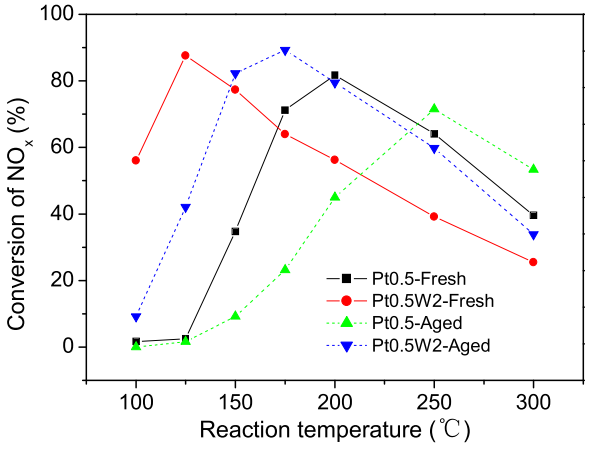


**Fig. 5.** Effect of hydrothermal aging on the $H_2$-SCR activities of Pt0.5 and Pt0.5W2 catalysts. Aging conditions: 5%$H_2O$/5%$O_2$/He at 700 °C for 4 h. Reaction conditions: 0.25% NO, 1% $H_2$, 5% $O_2$, He balance, GHSV = 53, 000 $h^{-1}$.

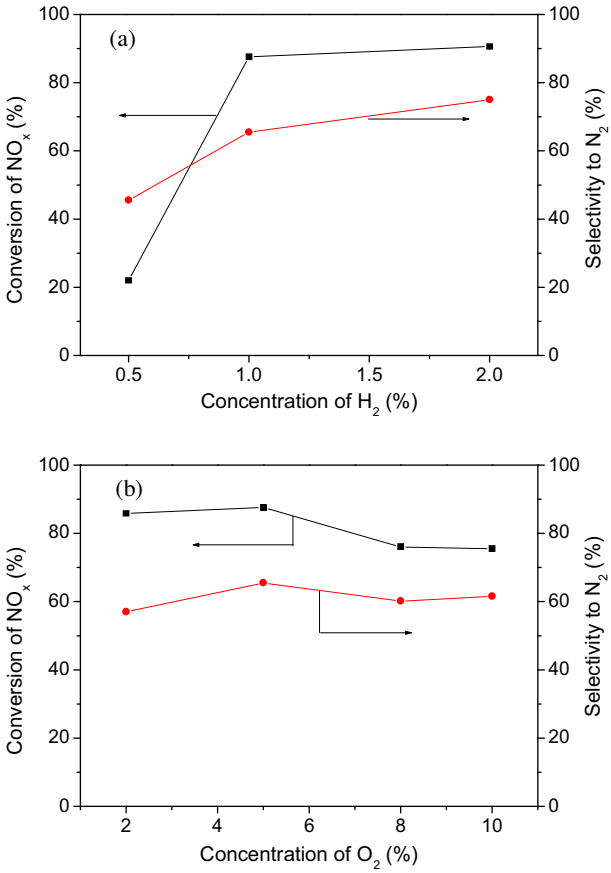


**Fig. 6.** Effects of $H_2$ (a) and $O_2$ (b) concentrations on $H_2$-SCR performance of Pt0.5W2 catalyst at 125 °C. Reaction conditions: 0.25% NO, 0.5–2% $H_2$, 2–10% $O_2$, He balance, GHSV = 53, 000 $h^{-1}$.

conversion of $NO_x$ almost remains constant with further increasing the $H_2$ concentration from 1% to 2%. This indicates that complete conversion of $NO_x$ was achieved at 125 °C after using a $H_2$/NO molar ratio of 4. Over Pt/MgO-$CeO_2$ catalyst, the molar ratio of $H_2$/NO is 15 for the complete conversion of $NO_x$ [13]. In view of the practical application, the economic factors should be considered and a lower $H_2$/$NO_x$ feed ratio was desirable to obtain a relatively high $NO_x$ conversion, which would result in better economic performance of the given $H_2$-SCR process. Therefore, the present Pt0.5W2 cat-

**Table 1**
BET surface area of different catalysts.

| Catalyst | Surface area ($m^2\ g^{-1}$) |
|---|---|
| Pt0.5 | 42 |
| Pt0.5W1 | 51 |
| Pt0.5W2 | 51 |
| Pt0.5W5 | 52 |

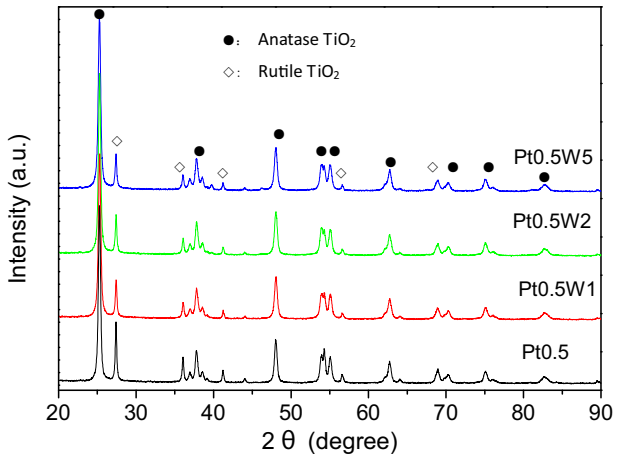


**Fig. 7.** XRD patterns of Pt0.5 and Pt0.5Wx catalysts.

alyst could appropriately reduce the usage of the reducing agent to obtain satisfactory treatment efficiency and greatly improve its economic performance.

As illustrated in Fig. 6(b), increasing $O_2$ concentration from 2% to 5% leads to the slight increase of $NO_x$ conversion and $N_2$ selectivity. Then an obvious decrease of $NO_x$ conversion can be observed with continuous increasing of $O_2$ concentration. These indicated that low concentration of $O_2$ can contribute to the oxidation of NO to $NO_2$, which is more active in the SCR of $NO_x$. With further increasing the concentration of $O_2$, the combustion of $H_2$ to form $H_2O$ was promoted, thus resulting in a decrease of the $NO_x$ conversion. This is in good accordance with the reported results on Pt/MgO-$CeO_2$ catalyst [13].

### 3.6. Catalyst characterization

#### 3.6.1. BET surface area and XRD patterns

The BET surface areas of Pt/$TiO_2$ catalyst with different $WO_3$ loading are summarized in Table 1. It can be seen that the introduction of $WO_3$ to Pt/$TiO_2$ leads to general increase of the BET surface area. The high specific surface area could contribute to the adsorption of $NO_x$, thus promoting the $H_2$-SCR of $NO_x$.

The XRD patterns of the Pt and PtW catalysts are presented in Fig. 7. Only the peaks assigned to the anatase and rutile form of $TiO_2$ were observed [29]. Both the peaks ascribed to Pt and $WO_3$ were absent. One reason is that these two species were highly dispersed on the surface of $TiO_2$, and the other one could be due to the limit of detection of the XRD. Compared with the single Pt catalyst, the intensity of the peak assigned to rutile $TiO_2$ ($2\theta = 27^\circ$) became weaker over PtW catalysts. This fact indicates that the addition of $WO_3$ can suppress the phase transformation of $TiO_2$ from anatase to rutile. Similar effect of $WO_3$ on $V_2O_5$/$TiO_2$ catalyst was also reported [30]. Anatase-phase $TiO_2$ possesses higher surface area than rutile-phase $TiO_2$ [30,31] and thus contributes to improving the $H_2$-SCR activity.

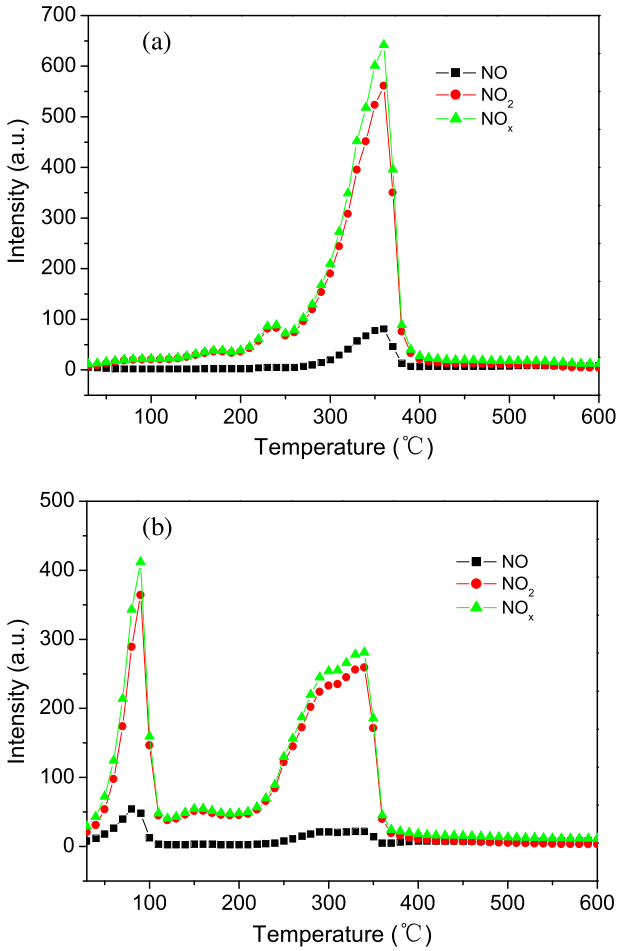


**Fig. 8.** $NO_x$-TPD profiles over Pt0.5 (a) and Pt0.5W2 (b) catalysts.

#### 3.6.2. $NO_x$-TPD

Fig. 8 illustrates the $NO_x$-TPD profiles over Pt0.5 and Pt0.5W2 catalysts. For Pt0.5 catalyst only one distinct desorption peak of $NO_x$ centered at about 350 °C was observed. The desorbed $NO_x$ is 198 $\mu mol\ g_{cat}^{-1}$, most of which is $NO_2$. In contrast, two desorption peaks of $NO_x$ at 90 and 340 °C appeared over Pt0.5W2 catalyst. The desorbed $NO_x$ are 76 and 123 $\mu mol\ g_{cat}^{-1}$, respectively. This fact indicates that new adsorbed species with less thermal stability formed due to the addition of $WO_3$. Since $NO_x$ ad-species formed on the catalyst surface is known to play an important role in $NO_x$ reduction [10], $NO_x$ adspecies desorbed at 90 °C are presumed to participate in the low temperature $NO_x$ reduction. $NO_2$, which is more active than NO, plays an important role in the SCR process. Ueda et al. [32] found that the reduction of $NO_2$ by $H_2$ is faster than the $O_2 + H_2$ reaction over the Pd/$TiO_2$ catalyst. From the $NO_x$-TPD results, it can be seen that the introduction of $WO_3$ contribute to the formation of $NO_2$ and its desorption. The noticeable higher $NO_x$ conversion over Pt0.5W2 catalyst could be attributed to the formation of more active $NO_2$ at low temperatures.

#### 3.6.3. $H_2$-TPR

TPR profiles of Pt0.5 and Pt0.5W2 catalysts are illustrated in Fig. 9. In the case of Pt0.5 catalyst, three hydrogen consumption peaks centered at around 173, 355 and 625 °C are present. The first peak was associated to the reduction of $PtO_x$ crystallites to metallic Pt [33–35], the latter two peaks at 355 and 625 °C could be attributed to the reduction of the surface capping oxygen of $TiO_2$ [34,35] and the reduction of bulk $TiO_2$ [34,36], respectively. For Pt0.5W2 catalyst, two reduction peaks centering at around 145

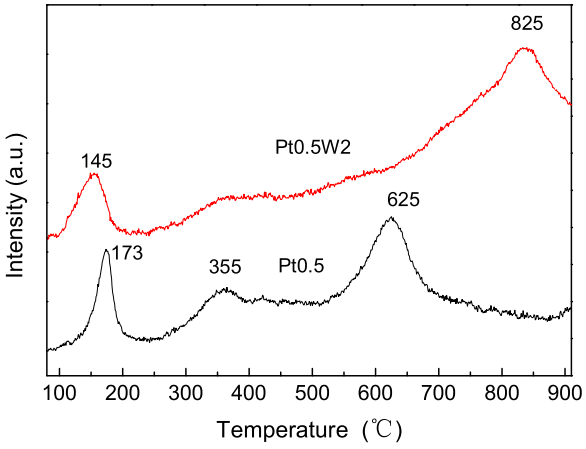


**Fig. 9.** $H_2$-TPR profiles of Pt0.5 and Pt0.5W2 catalysts.

and 825 °C are observed, which correspond to the reduction of $PtO_x$, and the co-reduction of $WO_3$ and $TiO_2$, respectively. The introduction of $WO_3$ to $Pt/TiO_2$ catalyst resulted in a weaker $PtO_x$ reduction peak and a shift of the peak to lower temperature, indicating that $PtO_x$ species becomes less and more reducible over Pt0.5W2. This could be responsible for the improvement of catalytic activity at low temperatures. The disappearance of the reduction peak at around 600 °C and the generation of new reduction peak at 825 °C suggest an interaction of $WO_3$ and $TiO_2$ exists in the meantime. This is in good accordance with the XRD results.

### 3.6.4. XAFS analysis

The position and the fine structure of the catalyst in an XANES spectrum are unique and sensitive, and are often used as fingerprint for the changes in valence of elements [37]. Generally, with the decreasing oxidation state, the absorption edge is shifted to lower energies [38]. Fig. 10(a) shows the Pt $L_2$ edge of Pt0.5, Pt0.5W2 and reference compounds Pt-foil and $PtO_2$. The first and (typically) most intense peak in a given XANES spectrum is often referred to as the "white line" of that absorption edge. The white line appears as a result of bound state transition between core electrons and the unoccupied valence states characteristic of the absorption edge [39]. In the case of the Pt $L_2$-edge, the white line represents a 2p–5d electronic transition, and therefore, its intensity is reflective of the occupation of the 5d orbitals; higher occupation results in lower white line intensity and vice versa. The shape of the near-edge region is sensitive to both the phase and oxidation state of the element of interest, and therefore, the identical fine structure between the Pt $L_2$-edge XANES spectra of the Pt0.5 and $PtO_2$ (shown in Fig. 10(a)) illustrates that the Pt species in Pt0.5 was present in $Pt^{4+}$ oxidation state. After doping W, the intensity of the white line became lower than that of Pt0.5 catalyst, indicating that an electron was transferred to Pt on Pt0.5W2 catalyst.

To further determine the average valence of Pt species in Pt0.5W2 catalyst, the first-order derivates of Pt $L_2$ XANES were taken and compared with Pt0.5 and the reference samples (see Fig. 10(b)). The red shift of Pt in Pt0.5W2 sample indicates that the valence of Pt was reduced from $Pt^{4+}$ to $Pt^0$. The electron configuration of $Pt^{4+}$ is [Xe] $4f^{14}5d^{5}6s^{1}$, while $Pt^0$'s is [Xe] $4f^{14}5d^{9}6s^{1}$. As shown in Fig. 10(b), the intensity of white line for Pt0.5W2 is reduced with the energy shifted to lower positions than Pt0.5, indicating that the valence state of Pt is reduced with the empty electron hole in 5d orbital decreased. All these characteristics show that the Pt species in Pt0.5W2 was partly reduced to the metallic state.

Fig. 11 illustrates the W $L_3$ edge of Pt0.5W2 and $WO_3$. Both of them have a broad white line with a FWHM about 10 eV, which

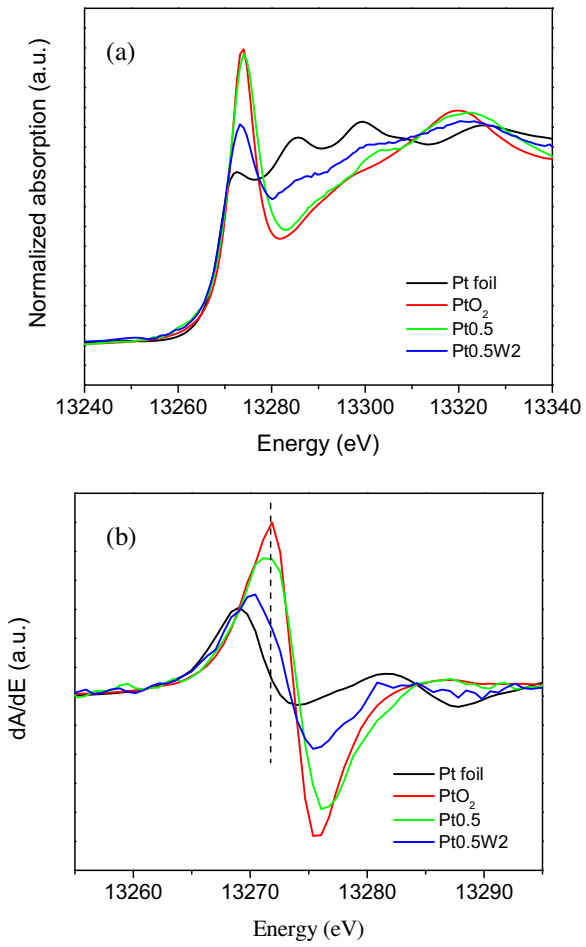


**Fig. 10.** Normalized XANES (a) and first-order derivates of XANES (b) of Pt $L_2$ edge of Pt0.5, Pt0.5W2 and reference samples.

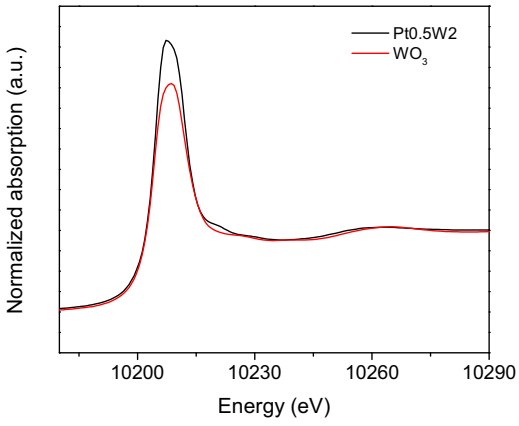


**Fig. 11.** Normalized XANES of W $L_3$ edge of Pt0.5W2 and $WO_3$.

suggests that $WO_3$ is in an octahedral oxide configuration [40]. Correlating with the changes of Pt $L_2$-edge XANES in Pt0.5W2, the increase of the peak intensity of W $L_3$ edge in Pt0.5W2 indicates that the electron was transferred to Pt from W, resulting in the increase of empty d electronic state, as shown in Fig. 10.

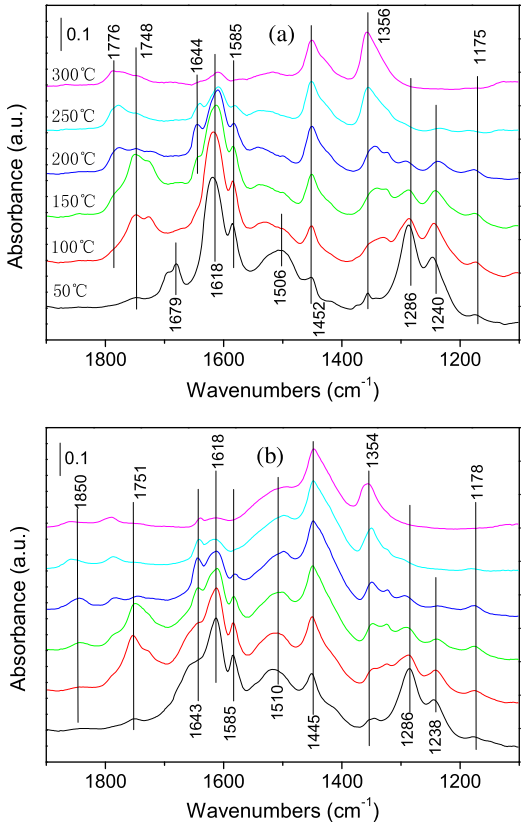


**Fig. 12.** In situ DRIFTS spectra of $NO + O_2$ adsorption on Pt0.5 (a) and Pt0.5W2 (b) catalysts at different temperatures. Conditions: 0.25% NO, 5% $O_2$, He balance.

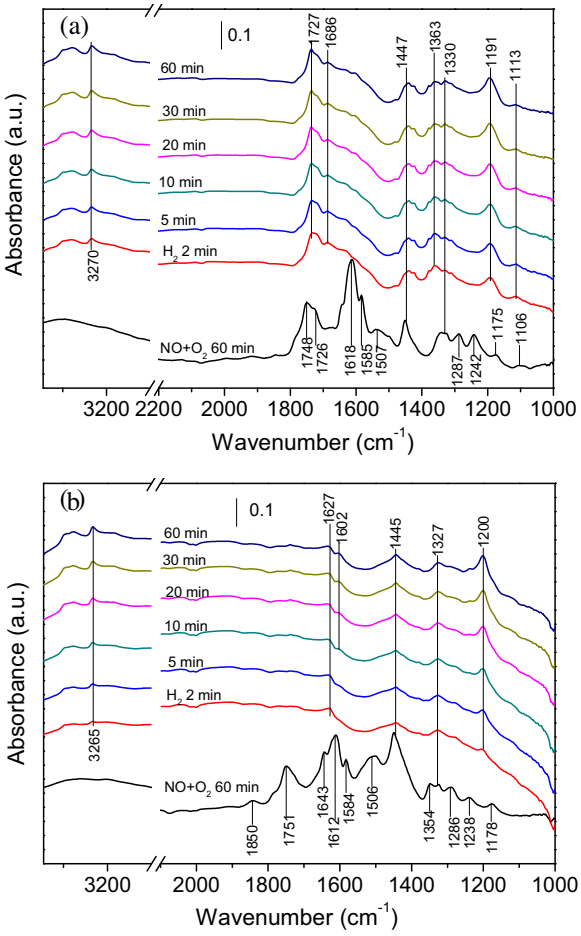


**Fig. 13.** Dynamic changes of the in situ DRIFT spectra over Pt0.5 (a) and Pt0.5W2 (b) catalysts in a flow of $H_2$ after the catalysts were pre-exposed to a flow of $NO + O_2$ for 60 min at 150 °C. Conditions: 0.25% NO, 1% $H_2$, 5% $O_2$, He balance.

### 3.7. *In situ DRIFT studies*

#### 3.7.1. *Co-adsorption of $NO + O_2$*

Fig. 12 compares the DRIFT spectra of $NO + O_2$ on Pt0.5 and Pt0.5W2 catalysts at different temperatures. Over Pt0.5 catalyst (see Fig. 12(a)), a series of distinct bands appeared at 1748, 1679, 1618, 1585, 1506, 1452, 1356, 1286, 1240 and 1175 $cm^{-1}$, which are respectively ascribed to *trans*-$(NO)_2$ (1748 $cm^{-1}$) [29], adsorbed NO (1679 $cm^{-1}$) [41], asymmetric vibration mode of adsorbed $NO_2$ (1618 $cm^{-1}$) [29,42], bidentate nitrate (1585 $cm^{-1}$) [41,43], monodentate nitrate (1506 and 1452 $cm^{-1}$) [10], chelating nitrite (1356, 1286 and 1175 $cm^{-1}$) [44,45] and monodentate nitrite species (1242 $cm^{-1}$) [41]. With increasing temperature, the peaks assigned to *cis*-$(NO)_2$ (1776 $cm^{-1}$) [29] and bridged nitrate (1643 $cm^{-1}$) [46] appeared. Over Pt0.5W2 catalyst (see Fig. 12(b)), the intensities of the peaks assigned to monodentate nitrate (1510 and 1445 $cm^{-1}$) and bridged nitrate (1643 $cm^{-1}$) become higher, indicating that the addition of $WO_3$ contributes to the formation of these species. Moreover, a new band due to $NO^{\delta+}$ on Pt (1850 $cm^{-1}$) [13] was observed. Therefore, addition of $WO_3$ to Pt0.5 not only led to more species adsorbed on the catalyst but also induced new species formed on the surface of the catalyst.

#### 3.7.2. *Reactivity of adsorbed $NO_x$*

The reactivity of adsorbed nitrogen oxides species in $H_2$-SCR reaction on Pt0.5 and Pt0.5W2 catalysts was investigated by performing a transient study and the results are shown in Fig. 13. Fig. 13(a) shows that on Pt0.5 catalyst after the gas flow was switched from $NO + O_2$ to $H_2$ at 150 °C, these bands assigned to $NO_2$ (1618 $cm^{-1}$), bidentate nitrate (1585 $cm^{-1}$) and monodentate nitrite (1242 $cm^{-1}$) decreased rapidly, and the intensity of the band related to monodentate nitrate (1506 and 1452 $cm^{-1}$) decreased gradually. These results suggest that these species are reaction intermediates in the reduction of $NO_x$ by $H_2$. The band ascribed to *trans*-$(NO)_2$ (1748 $cm^{-1}$) was shifted to 1727 $cm^{-1}$ and its intensity did not change significantly, indicating that it is spectator species for the $H_2$-SCR. Meanwhile, the bands due to symmetric and asymmetric bending vibrations of $NH_4^+$ on Brønsted acid sites (1686 and 1447 $cm^{-1}$) [43], and adsorbed $NH_3$ on Lewis acid sites (3270, 1363 and 1191 $cm^{-1}$) [47] appeared. It is noted that the peak position of monodentate nitrate is similar to that of $NH_4^+$ on Brønsted acid sites (1447 $cm^{-1}$).

As shown in Fig. 13(b), after the gas flow was switched from $NO + O_2$ to $H_2$ at 150 °C, these bands attributed to $NO^{\delta+}$ on Pt(1850 $cm^{-1}$), *trans*-$(NO)_2$ (1751 $cm^{-1}$), bridged nitrate (1643 $cm^{-1}$), $NO_2$ (1612 $cm^{-1}$), bidentate nitrate (1584 $cm^{-1}$), monodentate nitrate (1506 and 1445 $cm^{-1}$), chelating nitrite (1354, 1286 and 1178 $cm^{-1}$) and monodentate nitrite species (1238 $cm^{-1}$) exhibited a dramatic decrease in intensity and completely disappeared in 2 min. Subsequently, adsorbed $NH_4^+$ on Brønsted acid sites (1445 $cm^{-1}$) and coordinated $NH_3$ on Lewis acid sites (3265, 1327 and 1200 $cm^{-1}$) appeared. This fact demonstrated that almost all the adsorbed $NO_x$ species are reactive over Pt0.5W2 catalyst. Correlated with Fig. 12, it is evident that more reactive $NO_x$ species formed over Pt0.5W2 than Pt0.5 catalyst.

#### 3.7.3. *DRIFT spectra in a flow of $NO + H_2 + O_2$*

Fig. 14 illustrates the in situ DRIFT spectra of Pt0.5 and Pt0.5W2 catalysts at various temperatures under the steady-state condition after the reaction of $NO + H_2 + O_2$ for about 1 h. Over Pt0.5

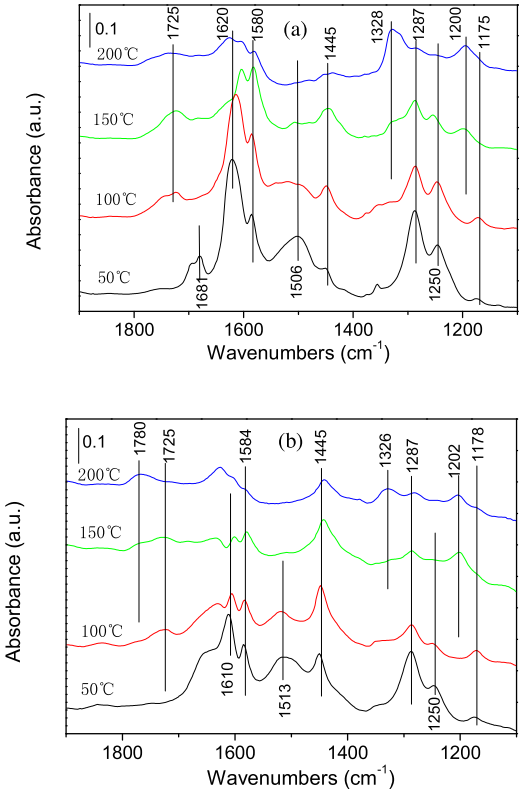


**Fig. 14.** In situ DRIFTS spectra of surface species in the steady state over Pt0.5 (a) and Pt0.5W2 (b) catalysts in the flow of 0.25%NO + 1%$H_2$ + 5%$O_2$. Conditions: 0.25% NO, 1% $H_2$, 5% $O_2$, He balance.

catalyst(see Fig. 14(a)), it can be seen that the intensities of the peaks ascribed adsorbed $NO_2$ (1620 $cm^{-1}$), bidentate nitrate (1580 $cm^{-1}$), chelating nitrite species (1287 $cm^{-1}$) and monodentate nitrite (1250 $cm^{-1}$) are still high with increasing temperature from 50 to 100 °C. As the temperature was increased to 150 °C, the bands related to adsorbed $NO_2$, chelating nitrite and monodentate nitrite species become weak. And the peak assigned to bidentate nitrate becomes weak only as the temperature was increased to 200 °C.

From Fig. 14(b), it can be seen that all the bands assigned to adsorbed $NO_x$ species over Pt0.5W2 were weaker than those observed over Pt0.5 catalyst. Even the temperature was increased from 50 to 100 °C, the intensities of the bands ascribed to adsorbed $NO_x$ species were noticeably decreased, indicating that the reaction between $NO_x$ and $H_2$ was promoted due to the addition of $WO_3$. From the comparison between Fig. 14(a) and (b), it is evident that the adsorbed $NO_x$ become significantly less over Pt0.5W2 catalyst. While from Fig. 12, it demonstrated that more adsorbed $NO_x$ formed when only feeding NO + $O_2$. These facts suggest that the formed nitrate, nitrite and $NO_2$ were quickly eliminated by the presence of $H_2$ over Pt0.5W2. It is well worthy to note that more $NH_4^+$ on Brønsted acid sites formed over Pt0.5W2 than Pt0.5 catalyst.

### 3.7.4. $NH_3$ adsorption

Surface acidity change of Pt0.5W2 due to $WO_3$ addition was studied by exposing Pt0.5 and Pt0.5W2 to $NH_3$ with increasing temperatures, and the DRIFT spectra are illustrated in Fig. S1. Over Pt0.5 catalyst the bands at 1594 and 1160 $cm^{-1}$ with shoulder at 1226 $cm^{-1}$ are assigned to asymmetric and symmetric bending vibrations of the coordinated $NH_3$ on Lewis acid sites[1,29], and those at 3367, 3260 and 3157 $cm^{-1}$ are ascribed to the N—H stretching vibration modes of the coordinated $NH_3$ [29]. The bands ascribed to asymmetric and symmetric bending vibrations of $NH_4^+$ species on Brønsted acid sites (1432 and 1667 $cm^{-1}$)[45,48] are also observed (see Fig. S1(a)). As shown in Fig. S1(b), stronger $NH_4^+$ (1665, 1478 and 1440 $cm^{-1}$) and $NH_3$ bands (3370, 3260, 3158, 1598 and 1183 $cm^{-1}$) are observed on Pt0.5W2 catalyst than those on Pt0.5 catalyst, indicating that the introduction of $WO_3$ leads to the increase of both Brønsted and Lewis acid sites on Pt0.5W2 catalyst. Shan et al. [48] also found that the addition of W to CeTi increased both the Brønsted and Lewis acid sites. The increased acidity of Pt0.5W2 catalyst contributes to the desorption of $NO_x$ at low temperatures as shown in Fig. 8.

### 3.8. Role of $WO_3$

The nature of noble metal was crucial for the high activity of $H_2$-SCR catalyst. Machida et al. [49] compared the catalytic performance of Pt/$TiO_2$-$ZrO_2$ pretreated by $H_2$ and $O_2$ at 400 °C and found that the activity of the oxidized catalyst is much lower than the reduced one. Nanba et al. [21] found that two active temperature regions existed over Pt/$Al_2O_3$ catalyst. The low and high temperature regions agree with those for reduced and oxidized Pt species respectively, indicating that the nature of the noble metal can affect the temperature window. The addition of $WO_3$ to Pt catalyst induced the reduction of Pt species, thus the activity temperature window was shifted to lower temperatures (see Fig. 1).

The surface diffusion (spillover) of H species from Pt to the support is very important for the $H_2$-SCR to proceed [10,12]. The reduced Pt could improve the surface coverage of hydrogen on its surface, and in turn the rate of H-spillover from Pt to the support interface, and thus the rate of $NO_x$ reduction [10]. Metallic Pt also contributes to improving the oxidation of NO to $NO_2$ [50]. The addition of $WO_3$ to Pt leads to the formation of $Pt^0$, thus contributing to the spillover of activated H and effectively improving the oxidation of NO to $NO_2$, as shown in the $NO_x$-TPD profiles (see Fig. 8).

Nitrate species was reported to be reactive in the $H_2$-SCR of $NO_x$ [8,51]. Nitrosyls and bidentate nitrate were found to be reaction intermediates on Pt/$La_{0.5}Ce_{0.5}MnO_3$ catalyst [52]. In the case of Pt/MgO-$CeO_2$ catalyst, below 200 °C two active $NO_x$ reaction intermediates were formed: bidentate or monodentate nitrate located on the MgO support and $NO^+$ coadsorbed with nitrate ($NO_3^-$) species on an adjacent metal cation-oxygen anion site pair on $CeO_2$ [41]. The addition of $WO_3$ to Pt0.5 not only leads to the formation of more monodentate nitrate and bridged nitrate species but also a new species $NO^{\delta+}$ on Pt produced on the catalyst (see Fig. 12). $NO_x$-TPD result suggests the decreased binding energy between the adsorbed $NO_x$ species and the surface of Pt0.5W2, on which the species was unstable and prone to reacting with the activated H atoms. Transient DRIFTS studies also showed that over PtW catalyst the adsorbed $NO_x$ species are more reactive than those over single Pt catalyst in the $H_2$-SCR of $NO_x$ (see Fig. 13). Over Pt0.5 catalyst, *trans*-$(NO)_2$ is a spectator species as shown in Fig. 13. The spectator species would cover the Pt sites and prevent the activation of H and its spillover to the support, resulting in the low $H_2$-SCR activity.

Costa et al. [10] pointed out that the structure of adsorbed $NO_x$ and their binding energy with catalyst are key factors that control the activity of the $H_2$-SCR catalyst. The relatively lower binding energy of adsorbed $NO_x$ with catalyst would contribute to the desirable reaction with H atom and inhibited the activated H atom consumption by excess oxygen, thus leading to more active Pt sites occupied by hydrogen and facilitating the $H_2$-SCR reaction to proceed. The synergetic effect between Pt and $WO_3$ could promote the H-spillover from Pt to $WO_3$ and the support, resulting in the faster reaction rate of $H_2$ with adsorbed $NO_x$ (see Fig. 13). In addition, more $NH_4^+$ formed over Pt0.5W2 than Pt0.5 catalyst. Previous research showed that $NH_4^+$ species are key intermediate for $H_2$-SCR over Pt-based catalyst [17,53]. $WO_3$ was reported to be active

for $NH_3$-SCR of $NO_x$ [54,55]. Therefore, over Pt0.5W2 catalyst the reaction between $NH_4^+$ and $NO_x$ would become faster due to the presence of $WO_3$. In summary, the addition of $WO_3$ to Pt catalyst not only contributes to the formation of adsorbed $NO_x$ species on the catalyst but also enhanced their reactivity with $H_2$. Moreover, the promotion of $NH_4^+$ species formation and its reactivity should be another reason for the promoting effect of $WO_3$. All of these contribute to the high activity of PtW catalyst for the $H_2$-SCR of $NO_x$.

## 4. Conclusions

A novel $WO_3$ promoted $Pt/TiO_2$ has been developed for the selective catalytic reduction of $NO_x$ by $H_2$ in the presence of oxygen. The activity of $Pt/TiO_2$ catalyst at temperatures representative of automotive "cold-start" conditions can be significantly enhanced by the addition of $WO_3$, and the optimum $WO_3$ loading is 2%. In the presence of $H_2O$, the promoting effect of $WO_3$ is more noticeable. The presence of CO or $CO_2$ leads to the activity loss of $Pt/TiO_2$ catalyst, but $Pt\text{-}WO_3/TiO_2$ catalyst still exhibited relatively high de$NO_x$ activity. XANES results revealed that part of Pt species over $Pt\text{-}WO_3/TiO_2$ was present in the form of metallic Pt due to the introduction of $WO_3$. In-situ DRIFTS revealed that more adsorbed $NO_x$ species and $NH_4^+$ appeared. The synergetic effect between Pt and $WO_3$ not only led to the unstable adsorbed $NO_x$ species but also promoted the spillover of activated H. As a result, the removal of $NO_x$ over $Pt\text{-}WO_3/TiO_2$ catalyst was facilitated.

## Acknowledgments

This research was financially supported by the National Natural Science Foundation of China (21377010), the Fundamental Research Funds for the Central Universities (YS1401), State Environmental Protection Key Laboratory of Sources and Control of Air Pollution Complex (SCAPC201402), and the Program for New Century Excellent Talents of the Chinese Ministry of Education (NCET-13-0650).

## Appendix A. Supplementary data

Supplementary data associated with this article can be found, in the online version, at http://dx.doi.org/10.1016/j.apcatb.2016.02.008.

## References

[1] Z. Liu, S. Zhang, J. Li, J. Zhu, L. Ma, Appl. Catal. B 158–159 (2014) 11–19.
[2] Z. Liu, S.I. Woo, Catal. Rev. Sci. Eng. 48 (2006) 43–89.
[3] L. Ström, P. Carlsson, M. Skoglundh, H. Härelind, Appl. Catal. B 181 (2016) 403–412.
[4] F. Gao, M. Kollár, R.K. Kukkadapu, N.M. Washton, Y. Wang, János Szanyi, C.H.F. Peden, Appl. Catal. B 164 (2015) 407–419.
[5] N. Usberti, M. Jablonska, M.D. Blasi, P. Forzatti, L. Lietti, A. Beretta, Appl. Catal. B 179 (2015) 185–195.
[6] P.S. Kim, M.K. Kim, B.K. Cho, I.S. Nam, S.H. Oh, J. Catal. 301 (2013) 65–76.
[7] P.M. More, D.L. Nguyen, P. Granger, C. Dujardin, M.K. Dongare, S.B. Umbarkar, Appl. Catal. B 174–175 (2015) 145–156.
[8] Z. Liu, J. Li, S.I. Woo, Energy Environ. Sci. 5 (2012) 8799–8814.
[9] R.C. Hahn, M. Endisch, F.J.P. Schott, S. Kureti, Appl. Catal. B 168-169 (2015) 429–440.
[10] C.N. Costa, A.M. Efstathiou, J. Phys. Chem. C 111 (2007) 3010–3020.
[11] F. Gunnarsson, M.Z. Granlund, M. Englund, J. Dawody, L.J. Pettersson, H. Härelind, Appl. Catal. B 162 (2015) 583–592.
[12] P.G. Savva, C.N. Costa, Catal. Rev. Sci. Eng. 53 (2011) 91–151.
[13] C.N. Costa, P.G. Savva, J.L.G. Fierro, A.M. Efstathiou, Appl. Catal. B 75 (2007) 147–156.
[14] L. Li, P. Wu, Q. Yu, G. Wu, N. Guan, Appl. Catal. B 94 (2010) 254–262.
[15] F.J.P. Schott, P. Balle, J. Adler, S. Kureti, Appl. Catal. B 87 (2009) 18–29.
[16] J. Yang, O. Fu, D. Wu, S. Wang, Appl. Catal. B 49 (2004) 61–65.
[17] Q. Yu, M. Richter, L. Li, F. Kong, G. Wu, N. Guan, Catal. Commun. 11 (2010) 955–959.
[18] K. Yokota, M. Fukui, T. Tanaka, Appl. Surf. Sci. 121–122 (1997) 273–277.
[19] R. Burch, M.D. Coleman, J. Catal. 208 (2002) 435–447.
[20] M. Machida, T. Watanabe, Appl. Catal. B 52 (2004) 281–286.
[21] T. Nanba, C. Kohno, S. Masukawa, J. Uchisawa, N. Nakayama, A. Obuchi, Appl. Catal. B 46 (2003) 353–364.
[22] S. Zhou, B. Varughese, B. Eichhorn, G. Jackson, K. McIlwrath, Angew. Chem. Int. Ed. 44 (2005) 4539–4543.
[23] C.N. Costa, P.G. Savva, C. Andronikou, P.S. Lambrou, K. Polychronopoulou, V.C. Belessi, V.N. Stathopoulos, P.J. Pomonis, A.M. Efstathiou, J. Catal. 209 (2002) 456–471.
[24] C.N. Costa, A.M. Efstathiou, Appl. Catal. B 72 (2007) 240–252.
[25] G.L. Chiarello, D. Ferri, J.D. Grunwaldt, L. Forni, A. Baiker, J. Catal. 252 (2007) 137–147.
[26] M. Magnusson, E. Fridell, H.H. Ingelsten, Appl. Catal. B 111–112 (2012) 20–26.
[27] A. Väliheikki, K.C. Petallidou, C.M. Kalamaras, T. Kolli, M. Huuhtanen, T. Maunula, R.L. Keiski, A.M. Efstathiou, Appl. Catal. B 156–157 (2014) 72–83.
[28] R. Burch, M.D. Coleman, Appl. Catal. B 23 (1999) 115–121.
[29] Z. Liu, S. Zhang, J. Li, L. Ma, Appl. Catal. B 44 (2014) 90–95.
[30] G. Busca, L. Lietti, G. Ramis, F. Berti, Appl. Catal. B 18 (1998) 1–36.
[31] C. Liu, L. Chen, J. Li, L. Ma, H. Arandiyan, Y. Du, J. Xu, J. Hao, Environ. Sci. Technol. 46 (2012) 6182–6189.
[32] A. Ueda, T. Nakao, M. Azuma, T. Kobayashi, Catal. Today 45 (1998) 135–138.
[33] P. Panagiotopoulou, A. Christodoulakis, D.I. Kondarides, S. Boghosian, J. Catal. 240 (2006) 114–125.
[34] C. Zhang, H. He, K. Tanaka, Appl. Catal. B 65 (2006) 37–43.
[35] W.S. Epling, P.K. Cheekatamarla, A.M. Lane, Chem. Eng. J. 93 (2003) 61–68.
[36] X.Y. Jiang, G.H. Ding, L.P. Lou, Y.X. Chen, X.M. Zheng, J. Mol. Catal. A 218 (2004) 187–195.
[37] P. Li, Y. Xin, Q. Li, Z. Wang, Z. Zhang, L. Zheng, Environ. Sci. Technol. 46 (2012) 9600–9605.
[38] G. Zhang, F. Liu, H. Liu, J. Qu, R. Liu, Environ. Sci. Technol. 48 (2014) 10316–10322.
[39] S. Wang, D. Zhang, Y. Ma, H. Zhang, J. Gao, Y. Nie, X. Sun, ACS Appl. Mater. Interfaces 6 (2014) 12429–12435.
[40] S. Yamazoe, Y. Hitomi, T. Shishido, T. Tanaka, J. Phys. Chem. C 112 (2008) 6869–6879.
[41] S. Yang, C. Wang, J. Li, N. Yan, L. Ma, H. Chang, Appl. Catal. B 110 (2011) 71–80.
[42] Y. Peng, C. Wang, J. Li, Appl. Catal. B 144 (2014) 538–546.
[43] F.D. Liu, H. He, Y. Ding, C.B. Zhang, Appl. Catal. B 93 (2009) 194–204.
[44] P.G. Savva, A.M. Efstathiou, J. Catal. 257 (2008) 324–333.
[45] Z. Liu, J. Zhu, J. Li, L. Ma, S.I. Woo, ACS Appl. Mater. Interfaces 6 (2014) 14500–14508.
[46] S. Yang, X. Wang, W. Chu, Z. Song, S. Zhao, Appl. Catal. B 107 (2011) 380–385.
[47] Z. Liu, Y. Li, T. Zhu, H. Su, J. Zhu, Ind. Eng. Chem. Res. 53 (2014) 12964–12970.
[48] W. Shan, F. Liu, H. He, X. Shi, C. Zhang, Appl. Catal. B 115–116 (2012) 100–106.
[49] M. Machida, S. Ikeda, D. Kurogi, T. Kijima, Appl. Catal. B 35 (2001) 107–116.
[50] S.S. Mulla, N. Chen, L. Cumaranatunge, G.E. Blau, D.Y. Zemlyanov, W.N. Delgass, W.S. Epling, F.H. Ribeiro, J. Catal. 241 (2006) 389–399.
[51] K. Duan, B. Chen, T. Zhu, Z. Liu, Appl. Catal. B 176 (2015) 618–626.
[52] C.N. Costa, A.M. Efstathiou, J. Phys. Chem. B 108 (2004) 2620–2630.
[53] J. Shibata, M. Hashimoto, K. Shimizu, H. Yoshida, T. Hattori, A. Satsuma, J. Phys. Chem. B 108 (2004) 18327–18335.
[54] Z. Liu, Y. Liu, Y. Li, H. Su, L. Ma, Chem. Eng. J. 283 (2016) 1044–1050.
[55] Y. Peng, K. Li, J. Li, Appl. Catal. B 140–141 (2013) 483–492.